Freie Universität Berlin

Title:

Deep-core photoionization of krypton atoms below and above 1s ionization threshold

＋

Author(s):

Boudjemia, N.; Jänkälä, K.; Püttner, Ralph; Gejo, T.; Journel, L.; Kohmura, Y.; Huttula, M.; Piancastelli, M. N.; Simon, M.; Oura, M.

Deep-core photoionization of krypton atoms below and above $1s$ ionization threshold

N. Boudjemia,[1] K. Jänkälä,[1] R. Püttner,[2] T. Gejo,[3, 4] L. Journel,[3, 5] Y.
Kohmura,[3] M. Huttula,[1] M. N. Piancastelli,[3, 5, 6] M. Simon,[3, 5] and M. Oura[3]

[1]*Nano and Molecular Systems Research Unit, University of Oulu, P.O. Box 3000, 90014 Oulu, Finland*[*]
[2]*Fachbereich Physik, Freie Universität Berlin, Arnimallee 14, D-14195 Berlin, Germany*
[3]*RIKEN SPring-8 Center, 1-1-1 Kouto, Sayo-cho, Sayo-gun, Hyogo 679-5148, Japan*
[4]*Graduate School of Materials Science, University of Hyogo, Kamigori-cho, Ako-gun, Hyogo 678-1297, Japan*
[5]*Sorbonne Université, CNRS, Laboratoire de Chimie Physique-Matière et Rayonnement, LCPMR, F-75005, Paris, France*
[6]*Department of Physics and Astronomy, Uppsala University, SE-75120 Uppsala, Sweden*
(Dated: March 17, 2021)

Electronic relaxation of atomic Kr below and above the $1s$ ionization threshold is investigated experimentally using hard X-ray photoelectron spectroscopy. The experimental results are interpreted with the aid of relativistic Dirac-Fock calculations. The 1s orbital core-hole lifetime is extracted and the satellites structures accompanying the photoelectron main line are assigned. Auger spectra recorded below and above the K-edge are also investigated. In particular, the Auger cascade originating from vacancies of different origin in the L-shell is analyzed in great detail. Competition between radiative KL versus nonradiative KLL Auger emission is emphasized.

I. INTRODUCTION

Availability of high-resolution hard X-ray radiation up to 51 keV at SPring-8 [1] in Japan has opened new avenues for the study of heavy atoms and molecules with hard X-ray photoelectron spectroscopy (HAXPES), which is a powerful technique for investigation of deep-core orbitals of different materials in gas phase [1] or condensed matter [2]. In heavy atoms, either isolated or embedded in a molecule, this new possibility to create a very deep-core hole via single-photon excitation or ionization enables direct studies of a multitude of interesting phenomena such as core-hole lifetime in the attosecond range [3, 4], direct observation of the relative weight of KL emission processes versus Auger relaxation [3] and partial charge redistribution within a molecule [4].

Photoionization dynamics of Kr atoms have been under intense investigation in the past. Studies have been conducted in the soft X-ray photon energy range, which has enabled investigation of valence photoionization, Auger decay spectra and formation of multiply charged Kr ions as a function of the photon energy above the $2p_{3/2}$ ionization threshold [5–8]. Several studies using lasers have been conducted, such as measurement of X-ray transitions of Kr clusters [9], and pump-probe studies to trace the M-shell decay dynamics [10] and excitation using the OMEGA laser at Laboratory for Laser Energetics to study Kr K-shell X-ray emission [11]. Kr has been also studied in very strong photon fields at free electron lasers where the focus was put to multiphoton ionization [12] and with synchrotron-based time-resolved X-ray microprobe experiments for the investigation of high-field orbital alignment [13]. However, HAXPES studies on Kr atoms following K-edge ionization

are scarce. High photon energy has been used to investigate nondipole effects in $1s$ photoionization [14] and XAS measurements have been performed for structural determination of hydrophobic hydration shell of Kr [15]. $L_{2,3}MM$ and $M_{4,5}NN$ Auger spectra have been reported using electron impact ionization [16]. In addition, calculated energy diagram for Kr*-Kr^{4+} states, showing the most prominent relaxation channels for neutral Kr and Kr ions have been reported by Oura et al [1]. To our knowledge, Kr relaxation mechanisms around the K-edge have not been reported before. In particular, no detail studies are available focusing on the Auger cascades below and above the 1s ionization threshold.

The present paper provides the results of measurements carried out for Kr 1s ionization and the subsequent $LXX, (X = M, N)$ Auger decay cascade in the electron kinetic energy range of 1.0-1.8 keV. The Auger spectrum was also studied below the K-edge. The observed spectral features for both photoelectron and Auger electron spectra are assigned with the aid of relativistic Dirac-Fock calculations, which show good agreement with the experimental observations. The results obtained from the analysis of the 1s photoelectron spectrum of Kr include 1s binding energy, lifetime of the 1s ionized state and its radiative versus non-radiative decay branching ratio. For the Auger decay we provide a detailed analysis of the spectra starting from $2p^{-1}$ initial states and including three decay steps going from Kr^{1+} up to Kr^{4+}.

II. EXPERIMENT

Experiments were carried out at the BL29XU undulator beamline of SPring-8 [17]. The Kr 1s photoelectron spectrum was recorded using 19992 eV photon energy, and the Auger spectrum was measured below and above the K-edge at about 13.0 keV and 16.5 keV photon energies. The spectra were measured using a Scienta Omicron SES-2002 hemispherical deflection energy analyser with

a Scienta Gc50 gas cell [19]. The target pressure out-side the gas cell was about 4.5×10^{-5} mbar during the measurements.

Energy resolution of the electron energy analyzer was 360 meV with a pass energy of 200 eV. The photon band-width was estimated to be 2.90 eV at the photon energy of 19992 eV. The kinetic energy scale of the spectrome-ter was calibrated using the Ne KLL, Ar KLL and Kr LLM Auger spectra [20]. The photon energy scale was calibrated via the $1s$ binding energy of Ar, Xe $1s$, $2p$ and Kr $1s$, $2p$ [21]. The uncertainty of the incident photon energy has been estimated to be 3.1 eV.

III. CALCULATIONS

The calculations were carried out using the Flexible Atomic Code (FAC) [22], which uses a relativistic Dirac-Fock-Slater multiconfiguration atomic structure frame-work [23]. In this method atomic state functions (ASFs) with the same total angular momentum, projection and parity are constructed as linear combinations of con-figuration state functions (CSFs) in jj-coupling scheme. CSFs are thus antisymmetrized linear combinations of N-electron Slater determinants. The one-electron wave functions in the determinants were solved in the average energy level scheme via the self-consistent field Dirac-Fock method [23]. Then the mixing coefficients for ASFs were solved by diagonalizing the total relativistic Hamil-tonian in the CSFs basis. In addition to the relativis-tic effects provided by the Hamiltonian, Breit interaction and quantum electrodynamics corrections such as self en-ergy and vacuum polarization were included systemati-cally via perturbation theory. These additional correc-tions are critical for correct prediction of $1s$ binding en-ergies in heavy atoms [24].

Calculations of the singly ionized states included $1s^{-1}$, $2s^{-1}$, and $2p^{-1}$ states for the main lines, as well as $1s^{-1}$ $4s^{-1}nl$ and $1s^{-1}$ $4p^{-1}nl$ ($nl = 5s/p$, $6s/p$ and $7s/p$) con-figurations for the satellite lines. Auger transitions in the kinetic energy range of 1.0-1.8 keV were calculated by including transitions from the $(2s2p)^{-1}$ and $(2s2p)^{-2}$ initial state, and states with charge up to Kr^{4+}. The calculations at each Auger step included all relevant en-ergetically allowed final states that can be constructed from the occupied orbitals, meaning MX doubly, MXX, LMX and LLX triply and $XXXX$ quadruply ionized states, where X stands for holes in the M or N shell. Note that the decay of these holes does not produce elec-trons in the kinetic energy region under discussion, but is needed to predict the widths and intensities of the ob-served lines correctly.

Radiative transition rates were calculated in dipole ap-proximation using the length gauge. Auger decay rates were calculated in the standard formulation, except for construction of continuum waves that were approximated near the nucleus by the shape of highly excited bound or-bitals [22]. The cross section for $1s$ photoionization and

its satellite structure was taken from Ref. [30].

IV. RESULTS AND DISCUSSION

### A. Krypton $1s$ photoelectron spectrum
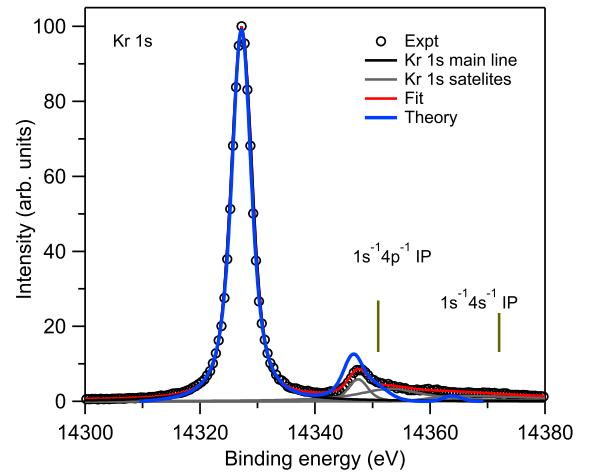
FIG. 1: Experimental and theoretical Kr $1s$ photoelectron spectrum. The $1s^{-1}4p^{-1}$ and $1s^{-1}4s^{-1}$ double ionization thresholds are indicated by vertical lines.

Figure 1 shows the experimental $1s$ photoelectron spec-trum of Kr measured at a photon energy of 19992 ± 3.1 eV. The $1s$ binding energy extracted from the spectrum is 14327 ± 3.2 eV, which is in agreement with the previ-ous literature values 14327.26 ± 0.4 eV and 14327.2 ± 0.8 eV [28, 29]. The value is also in good agreement with the present FAC calculations, which give the result of 14325.49 eV and previous calculation of 14326.10 eV ob-tained using the GRASP2K code [24].

The photoelectron spectrum in Fig. 1 was fitted us-ing four Voigt functions, one for the main line, three for the satellite structure. The energy positions of the satellites structures relative to the main line have been derived from the $2s$ photoelectron spectrum (not shown here). For the $1s$ main line the fit provides a full width at half maximum (FWHM) of 4.29 eV. Taking into account the instrumental broadening from the photon bandwidth (2.90 eV) and the electron analyzer broadening contribu-tion (0.36 eV), we determined the value of 2.22 ± 0.19 eV as width of the Lorentzian component. This corresponds to 295.5 ± 23 as for the lifetime of $1s$ ionized state of atomic Kr. The value is about 0.5 eV smaller than ob-served from Kr in aqueous solution (2.7 eV) [15] and from solid Kr (2.75 eV) [27].

Energy positions of the profiles peaks fitted to the satellite structures, with respect to the main line, were taken from the $2s$ photoelectron spectrum of Kr (not shown here), because the spectrum can be measured with

higher resolution. In the $1s$ case, the satellite spectrum has two distinct, but, due to the lifetime broadening, rather featureless regions approximately 20 eV and 35 eV from the main line. The first one is identified to transitions to $1s4p^{-1}nl$ final states and the second to $1s4s^{-1}nl$ final states. Table I provides the theoretical energy range for the $1s(4s4p)^{-1}ns, p$ satellite configurations. In general the present calculations for the energies combined with theoretical cross sections from [30] provide qualitative agreement with the measured $1s$ photoelectron spectrum.

TABLE I: Assignment and energy ranges of main satellite configurations. For each configuration the lowest and highest energy is given.

| | Energy ranges of satellites spectra in (eV) | | | |
| | Distance from threshold | | Binding energy | |
	Lowest value	Highest value	Lowest value	Highest value
$4p \to 5p$	18.61	21.23	14344.04	14346.66
$4p \to 6p$	22.58	24.04	14348.24	14349.70
$4p \to 7p$	24.14	25.39	14349.92	14351.17
$4s \to 5s$	36.57	37.73	14361.84	14363.00
$4s \to 6s$	42.08	42.97	14367.42	14368.32
$4s \to 7s$	44.12	44.98	14369.56	14370.41

B. Auger decay of Kr below and above $1s$ ionization threshold

Figure 2 shows the experimental and simulated Auger decay spectra in the electron kinetic energy range of 1075-1750 eV measured below (a) and above (b) the $1s$ ionization threshold. In this energy range only Auger decays of states that have at least one L hole contribute to the spectrum. The fundamental difference between the two spectra recorded below and above threshold is that the population of initial states is caused by different processes, as will be discussed below. As a result, below threshold the initial states have charge states of Kr^{1+} and Kr^{2+}, and exactly one hole in the L shell. Above threshold, on the other hand, the initial states range from Kr^{1+} to Kr^{3+} with a maximum of two holes in the L shell.

Below the $1s$ threshold initial states are produced solely by direct photoionization of the $L_{1,2,3}$-shells,

$$\gamma + Kr \xrightarrow{100\%} Kr^{1+}(2s2p)^{-1} + e_{ph}. \qquad (1)$$
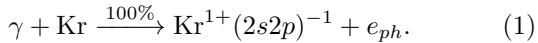
In contrast, above threshold the initial states are dominantly populated by, subsequent to K-shell photoionization, $KL_{2,3}$ X-ray emission, KLL and KLX Auger decay.

$$\gamma + Kr \xrightarrow{\sim 100\%} e_{ph} + Kr^{1+}(1s^{-1}) \qquad (2)$$
$$\xrightarrow{62\%} Kr^{1+}(2p^{-1}) + \gamma_{K\alpha}$$
$$\xrightarrow{29\%} Kr^{2+}(2s2p)^{-2} + e_{KLL}$$
$$\xrightarrow{9\%} Kr^{2+}((2s2p)^{-1}nl^{-1}) + e_{KLM}.$$
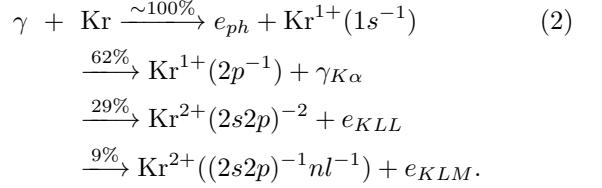
The decay probabilities for KL-fluorescence emission, KLL and KLX Auger yields of 62 %, 29 % and 9 % respectively are derived from the present calculation. Note that even though above threshold the $2s$ and $2p$ cross sections are non-zero, the $1s$ ionization cross section at 20 keV photon energy is 12, 53 and 30 times larger than the $2s$, $2p_{1/2}$ and $2p_{3/2}$ ionization cross sections, respectively. Therefore, the contribution of direct L-shell ionization can be neglected above the $1s$ threshold.

To understand the features of the spectra shown in Fig. 2 it is important to realize that the individual initial vacancies relax via different Auger cascades that produce overlapping features in the studied region. In the present case we included Auger steps up to quadruply ionized Kr, as will be discussed in detail in the following sections. Table II provides an electron configuration level summary of the possible Auger decay paths and their calculated kinetic energy ranges. In the following we shall discuss each initial decay step individually.

1. $Kr^{1+} \to Kr^{2+}$ Auger transitions

As mentioned above, Kr^+ ions with a hole in the L shell can be populated by process (1) and along the first two lines of process (2).

In Fig. 3 calculated partial Auger spectra associated with $Kr^{1+} \to Kr^{2+}$ transition are shown. The transition are further divided into different final-state components arising from the decay of $(2s2p)^{-1}$ vacancies below (top panel) and above (bottom panel) the $1s$ ionization threshold. Despite the different population mechanisms the two spectra are very similar since the $2s^{-1}$ hole decays predominantly via Coster-Kronig Auger decay which does not contribute in this energy region, see below. Note that the Coster-Kronig decay is a special Auger decay process where the created vacancy is occupied with an electron from the outer most subshell of the same shell. In the case where the emitted Auger electron belongs to the same shell, the process is called a super Coster-Kronig decay. The calculations include all energetically allowed Kr^{2+} configurations that can be constructed from the ground-state configuration of Kr. The calculations are in good agreement with the experiment. In particular, we predict all the spectral features, although only the major contributions to the peaks are shown in table II and Fig. 3. The main spectral features arise from filling the holes in the L-shell created by direct photoionization (below threshold) and by KL-emission (above threshold) leading to the doubly ionized
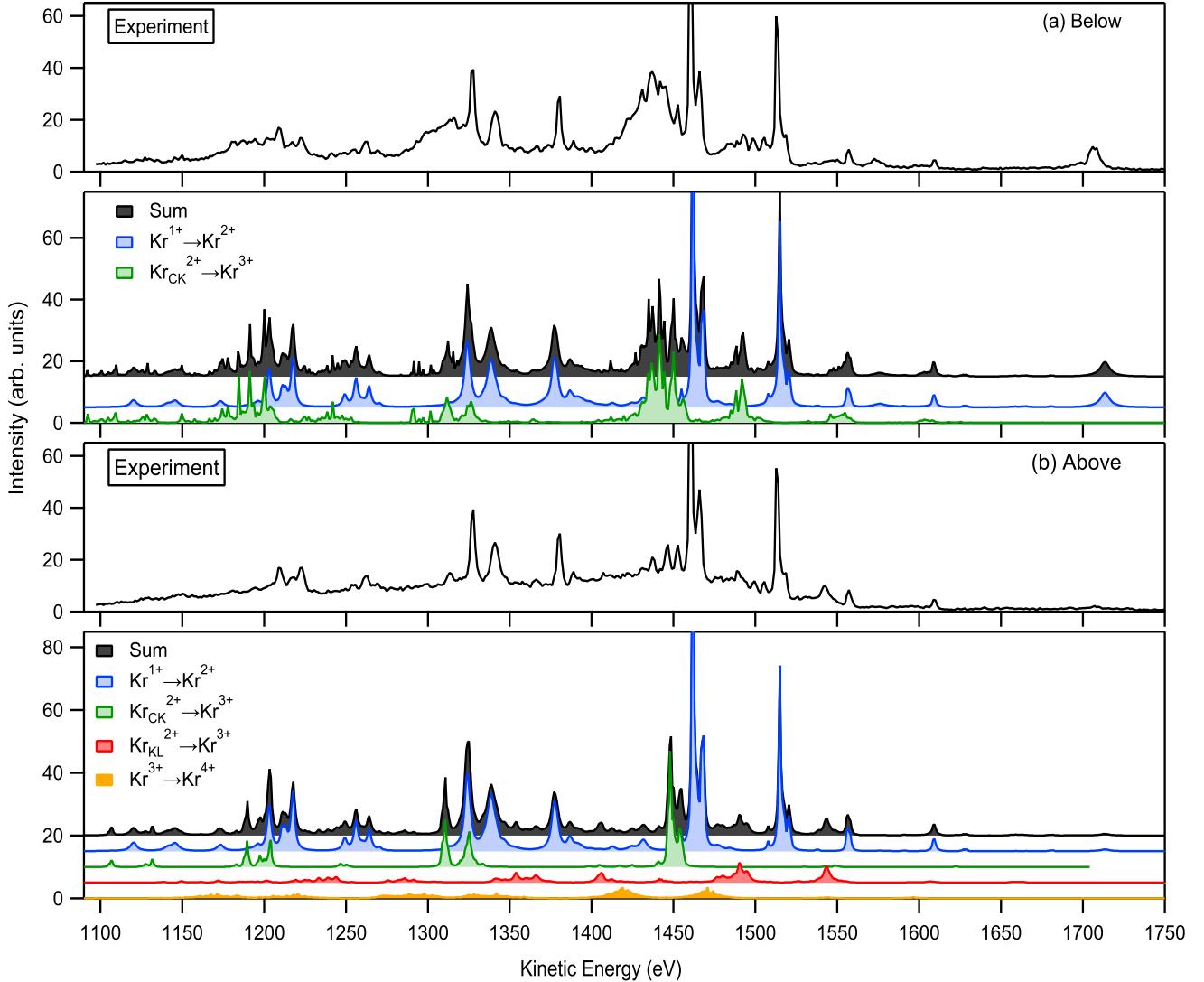
FIG. 2: Experimental and calculated Kr Auger decay spectra measured (a) below and (b) above $1s$ ionization threshold, showing total and partial contributions: $Kr^{n+} \rightarrow Kr^{m+}$. Kr_{CK}^{2+} (Kr_{KL}^{2+}) describes dicationic Kr states populated via LLX Coster-Kronig Auger decay (KLL and KLX Auger decay). The applied photon energies are 13.0 keV and 16.5 keV for below and above threshold, respectively. The spectra are normalized so that the most intense peak at 1460 eV is 100.

states $3p^4$, $3d^8$, $(3s3p3d)^{-1}4l^{-1}$, which can be found in the kinetic energy range of 1126-1744 eV. The $L_{2,3}MM$ structures have been reported before by Morishita *et al.* using a photon energy of 1850 eV [6]. The main colors of the sum spectra are the same as represented in the Fig. 2 in order to simplify comparison between the spectra below and above threshold.

Detailed comparison of the calculated LMX Auger spectra below and above threshold shows subtle variations in the relative intensities. In particular, the spectral feature at 1710 eV is strongly suppressed above threshold. It is assigned to L_1MX transition, whose initial state cannot be populated by KL-emission due to dipole selection rules.

The calculation of photoionization cross sections allowed us to support the observed behavior: between the two selected excitation photon energies 1.3 keV and 16.5 keV, the L-shell cross sections decrease by a factor of ~ 2. The $1s$ photoionization cross section at 16.5 keV photon energy is 12 times larger than the $2s$ cross section, 30 times larger than $2p_{3/2}$, and 53 times larger than $2p_{1/2}$. Consequently, the most intense LMX decays observed above threshold are due to the $KL_{2,3}$ fluorescence decay. In Fig. 3 the main features are similar between above and below threshold. The reason behind is that the most prominent features arise from the decay of $2p$ hole states, and KL_2/KL_3 fluorescence decay ratio as well as $2p_{1/2}/2p_{3/2}$ photoionization cross section ratio at
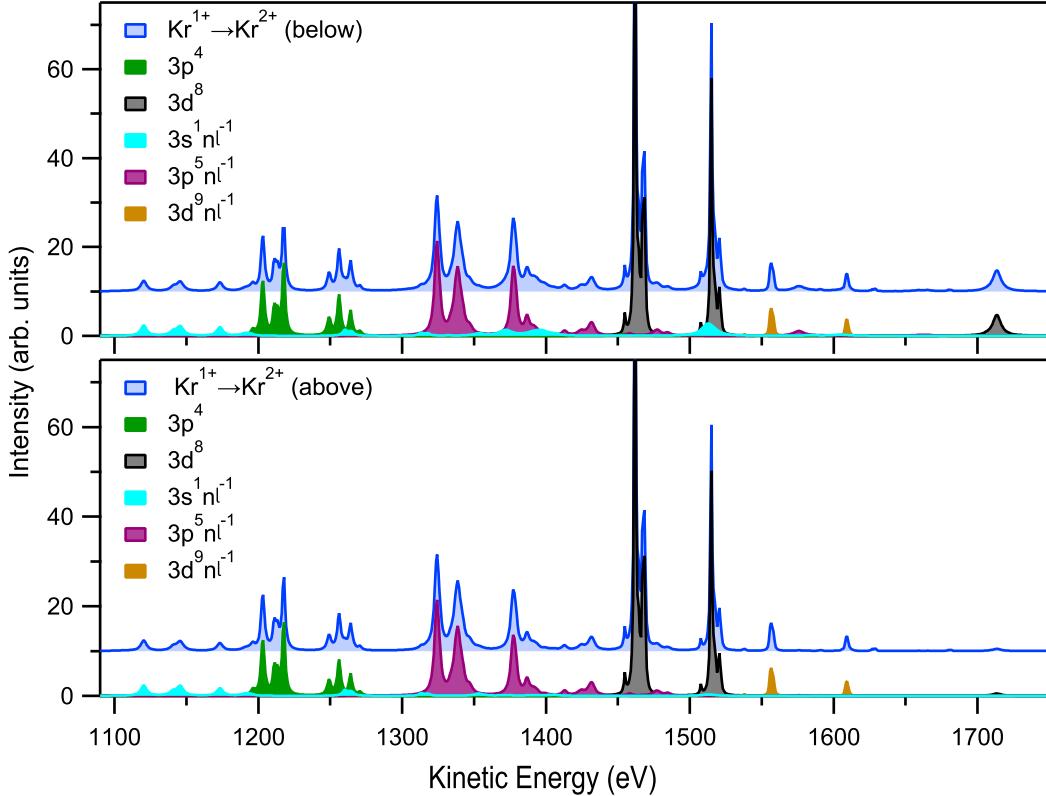
FIG. 3: Partial $Kr^{1+} \to Kr^{2+}$ contribution to total Auger spectrum below (top panel) and above (bottom panel) $1s$ ionization threshold. The different colors in the lower part of each panel indicate contribution of transitions to individual final-state configurations.

13 keV follow the statistical approximation of ~ 0.5.

The differences between the L-shell Auger spectra below and above the $1s$ threshold in Kr are similar to those which have been observed by Piancastelli *et al.* [3]. In Xe, however, the differences are more pronounced than in Kr. The reason for the differences is that $L_1 L_{2,3} M$ Coster-Kronig decays are intense in Kr, but due to energy conservation forbidden in Xe. This is reflected by the lifetime widths, see e.g. the ones of Krause and Oliver resulting in $\Gamma(L_1) = 4.28$, $\Gamma(L_2) = 1.31$, and $\Gamma(L_3) = 1.17$ for Kr, and $\Gamma(L_1) = 3.64$, $\Gamma(L_2) = 3.40$, and $\Gamma(L_3) = 3.13$ for Xe [27]. As a result the relative strength of $L_1 M X$ Auger transitions of the singly charged ion is weak in Kr but strong in Xe.

2. $Kr^{2+} \to Kr^{3+}$ *Auger transitions*

Assuming that contribution from direct double photoionization can be neglected, in the present experiment Kr^{2+} ions with holes in the L-shell can be obtained by two processes described in the following.

The first process is Coster-Kronig decay

$$Kr^{1+}(L_{1,2}) \to Kr^{2+}(L_{2,3}X) + e_{L_{1,2}L_{2,3}X}, \qquad (3)$$

where both $2s^{-1}$ and $2p_{1/2}^{-1}$ initial states are possible from direct photoionization; in addition $2p_{1/2}^{-1}$ initial states can be populated by KL_2 X-ray emission. The Coster-Kronig Auger spectra were not measured in the present experiment, but from the calculations it can be noted that the energy range of $L_1 L_{2,3} X$ Auger spectrum is at about 4-223 eV and $L_2 L_3 X$ at about 5-26 eV.

The second process to create Kr^{2+} ions with holes in $L_{1,2,3}$ shells is KLL and KLX Auger decay, i.e.

$$Kr^{1+}(K) \to Kr^{2+}(LL) + e_{KLL} \qquad (4)$$

and

$$Kr^{1+}(K) \to Kr^{2+}(LX) + e_{KLX}. \qquad (5)$$

These processes can occur only after $1s$ ionization. Also these electrons are not observed directly because, in contrast to the first process, their kinetic energies are well above the presently observed energy region. For example, calculated kinetic energy range of KLL Auger spectrum is in the range of 10.4-10.9 keV. Note that in process (4) $(2s2p)^{-2}$ states are created. Their sequential decay leads to the observation of Kr^{4+} final states, as will be discussed below.

TABLE II: Electronic configurations of initial and final states of Kr Auger decay measured below and above 1s ionization threshold ($n=3$ or 4).

Transition	Initial config	Final config	Kinetic energy (eV)
$\mathrm{Kr}^{1+} \to \mathrm{Kr}^{2+}$	$(2s2p)^{-1}$	$3p^4$	1129-1494
		$3d^8$	1430-1744
		$3s^1nl^{-1}$	1226-1711
		$3p^5nl^{-1}$	1226-1691
		$3d^9nl^{-1}$	1514-1635
$\mathrm{Kr}^{2+}_{CK} \underset{\longrightarrow}{below} \mathrm{Kr}^{3+}$	$2p^5nl^{-1}$	$3d^7$	1400-1514
		$3d^8nl^{-1}$	1425-1634
		$3s^13p^5nl^{-1}$	1073-1365
		$3p^4nl^{-1}$	1077-1442
		$3p^53d^9nl^{-1}$	1291-1571
$\mathrm{Kr}^{2+}_{CK} \underset{\longrightarrow}{above} \mathrm{Kr}^{3+}$	$2p^54p^5$	$3s^13p^54p^5$	1099-1139
		$3p^44p^5$	1175-1207
		$3s^13d^94p^5$	1238-1258
		$3p^53d^94p^5$	1302-1344
		$3d^84p^5$	1433-1460
$\mathrm{Kr}^{2+}_{LL} \to \mathrm{Kr}^{3+}$	$2p^4$	$2p^53p^4$	1140-1343
		$2p^53d^8$	1409-1614
		$2p^53s^1nl^{-1}$	1090-1486
		$2p^53p^5nl^{-1}$	1260-1570
		$2p^53d^9nl^{-1}$	1527-1715
$\mathrm{Kr}^{2+}_{LX} \to \mathrm{Kr}^{3+}$	$2p^5nl^{-1}$	$3p^3$	1127-1220
		$3d^7$	1409-1517
		$3p^43d^9$	1130-1600
		$3p^44s^1$	1158-1417
		$3p^43p^5$	1164-1443
		$3d^84s^1$	1418-1511
		$3d^84p^5$	1423-1610
$\mathrm{Kr}^{3+} \to \mathrm{Kr}^{4+}$	$2p^5nl^{-2}$	$3p^3nl^{-1}$	1128-1510
		$3p^43d^9nl^{-1}$	1230-1378
		$3p^4nl^{-2}$	1122-1527
		$3p^53d^8nl^{-1}$	1366-1505
		$3p^5nl^{-3}$	1232-1384
		$3d^7nl^{-1}$	1377-1505
		$3d^8nl^{-2}$	1491-1633
		nl^{-4}	1382-1725
		$3s^13d^8nl^{-1}$	1295-1416

Although the initial states are partially the same, we discuss the spectra of Auger decays of Kr^{2+} states created by Coster-Kronig decay and $KLL + KLX$ Auger decay separately. For this purpose the spectra are labelled as Kr^{2+}_{CK} and Kr^{2+}_{KL}, respectively.

3. $\mathrm{Kr}^{2+}_{CK} \to \mathrm{Kr}^{3+}$ Auger transitions

In Fig. 4 the partial Auger spectra associated to the transitions of $\mathrm{Kr}^{2+}_{CK} \to \mathrm{Kr}^{3+}$ measured below and above the 1s threshold are shown. The spectrum is separated into components indicated by different colors defined by the final-state electron configuration. The transitions in the upper panel (below threshold) arise from the decay of $2p^5nl^{-1}$ initial states populated by Coster-Kronig decay subsequent to direct L_1 and L_2 photoionization, where nl stands for $3p$, $3d$, $4s$ and $4p$. In the lower panel (above threshold) the intensities are predominantly due to Coster-Kronig decay after X-ray fluorescence so that the possible initial states are only $2p^5_{3/2}4s^{-1}$ and $2p^5_{3/2}4p^{-1}$.

States $2p^5nl^{-1}$ undergo further Auger relaxation of the type $\mathrm{Kr}^{2+}_{CK} \to \mathrm{Kr}^{3+} + e_{LXX}$ to triply ionized states giving rise to final states which lie in the kinetic energy of 1099-1711 eV and are detailed in the Table II, where nl represents singly or doubly ionized possible orbitals with $n = 3$, 4. In summary, the significant differences in the spectra are due to the reduced number of relevant initial-state configurations above threshold as a result of the X-ray fluorescence.

4. $\mathrm{Kr}^{2+}_{KL} \to \mathrm{Kr}^{3+}$ Auger transitions

Figure 5 shows the Auger decay of the Kr^{2+} ions with the L holes populated by the second process subsequent to ionization, KLL and KLX Auger transitions as described in Eq. (2). These Auger decays lead to the creation of Kr^{3+} ion according to

$$\mathrm{Kr}^{2+}(LL) \to \mathrm{Kr}^{3+}(LXX) + e_{LL-LXX} \qquad (6)$$

and

$$\mathrm{Kr}^{2+}(LX) \to \mathrm{Kr}^{3+}(XXX) + e_{LX-XXX}, \qquad (7)$$

where X stands for M or N.

The $\mathrm{Kr}^{3+}(LXX)$ still possess a hole in the L shell and can decay to Kr^{4+} by emitting an electron into the energy region under present investigation. Our calculation reveals that the second-step process leading to the production of $LL - LXX$ and $LM - MXX$ double core-hole hypersatellite structures is more important than in the case of 1s ionization of Xe [3]. This is due to the fact that in Kr the KLL and KLX-emission yields are calculated to be about 29 % and 9 % respectively, in contrast to Xe were KLL and KLX Augers combine to a decay probability of about 10 %.

Figure 5 shows the partial Auger spectrum of the $\mathrm{Kr}^{2+}_{KL}(LL) \to \mathrm{Kr}^{3+}$ transition, associated mainly to the decay of $2p^4$ initial states leading to $2p^5nl^{-2}$ or $2p^5n'l'^{-1}nl^{-1}$ final states. Here n and n' are predominantly equal to 3, i.e. the L-hole decays mainly by LMM Auger.
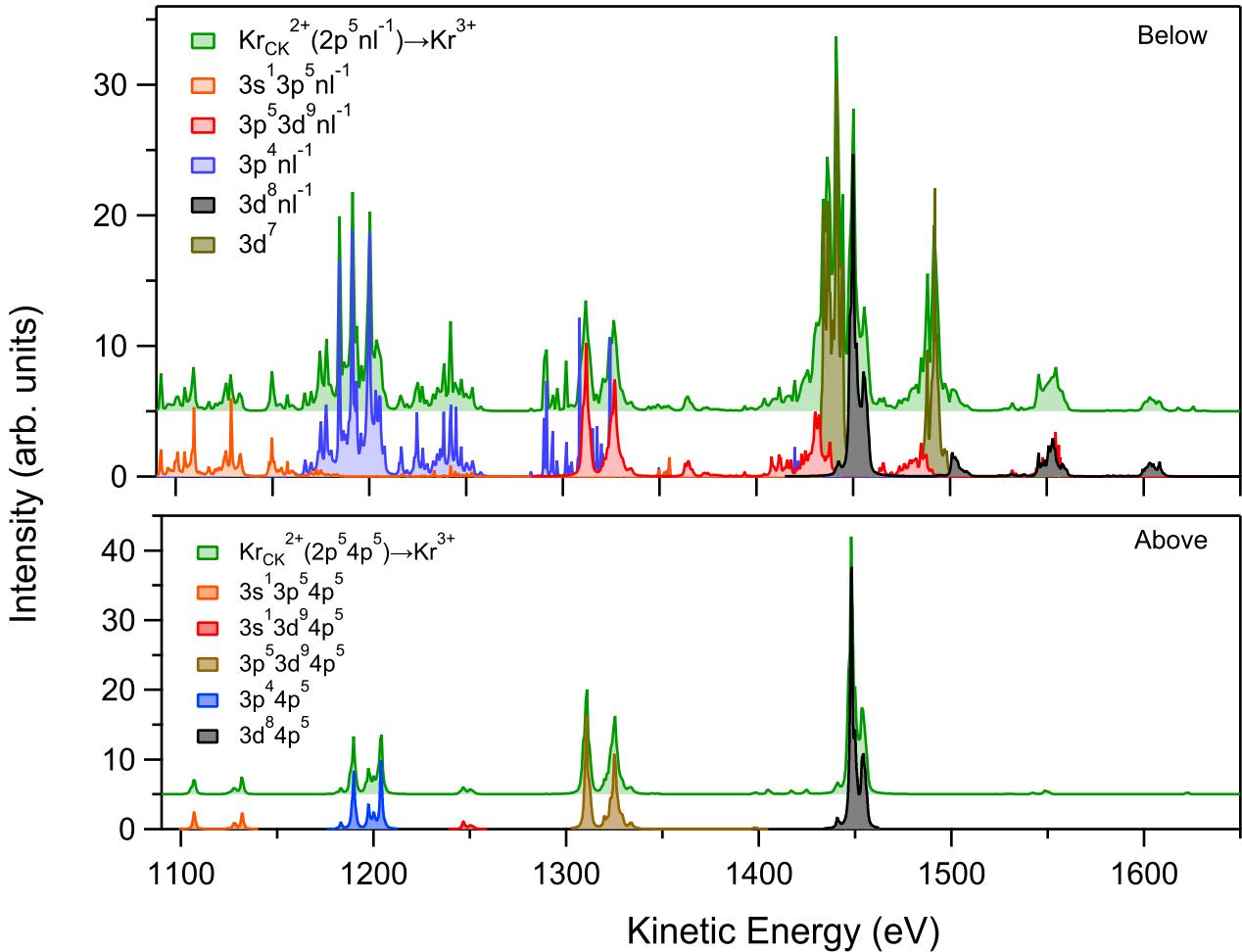
FIG. 4: Partial $\text{Kr}^{2+}_{CK} \to \text{Kr}^{3+}$ contribution to the Auger spectrum below and above $1s$ ionization threshold. The different colors in the lower part of each panel indicate contribution of transitions to individual final-state configurations.

As states above, $1s$ core-hole state decays via KLL Auger decay with 29 % probability. To be more specific, 18 % decay to $2p^4$, 8 % to $2s^1 2p^5$ and 3 % to $2s^0$ configurations. Because of low relative populations of $2s^1 2p^5$ and $2s^0$ states, their Auger spectra are not shown in Fig. 5. Note also that, since the states of the two latter configurations decay predominately via Coster-Kronig processes, their contribution to the $\text{Kr}^{2+}(LL) \to \text{Kr}^{3+}$ Auger spectrum is significantly smaller than their percentages in populating the $\text{Kr}^{2+}(LL)$ states.

Configurations of the final states of these Auger decays are presented in Table II. These structures are seen only above the K-edge threshold, such as the structures at kinetic energies of 1490 and 1540 eV, which have been assigned by our calculation to be $2p^4 \to 2p^5 3d^8$ transitions. The present spectra are in a good agreement with values predicted with a smaller-scale calculations by Oura *et al.* [1]. For the sake of visibility the $\text{Kr}^{2+}(LM) \to \text{Kr}^{3+}$ spectrum in Fig. 5 is multiplied by a factor of 5. The intensity of the $\text{Kr}^{2+}(LM) \to \text{Kr}^{3+}$ spectra multiplied by

a factor of 5 is shown in Fig. 3. Its multiplied intensity is comparable to the intensity of the $\text{Kr}^{2+}(LL) \to \text{Kr}^{3+}$ transitions. This can readily be understood by taking into account that the $\text{Kr}^{2+}(LL)$ to $\text{Kr}^{2+}(LX)$ population ratio is $\cong 3 : 1$ and that that in the case of $\text{Kr}^{2+}(LL)$ two L-holes can decay in contrast to $\text{Kr}^{2+}(LX)$ with only one hole in the L-shell.

Finally we shall compare the Auger energies. The energies of the $\text{Kr}^{2+}(LL) \to \text{Kr}^{3+}$ are generally larger than those of the $\text{Kr}^{2+}(LM) \to \text{Kr}^{3+}$ Auger transitions. This is probably due to the larger Coulomb repulsion of the two holes in the L shell than for one hole in the L and one in the X shell. This difference is in case of a $\text{Kr}^{2+}(LL$ initial state also transferred to the Auger electron.

5. $\text{Kr}^{3+} \to \text{Kr}^{4+}$ *Auger transitions*

As discussed above, the $\text{Kr}^{3+}(LXX)$ ions with a hole in the L-shell are created by the decay of $\text{Kr}^{2+}(LL)$ ions.
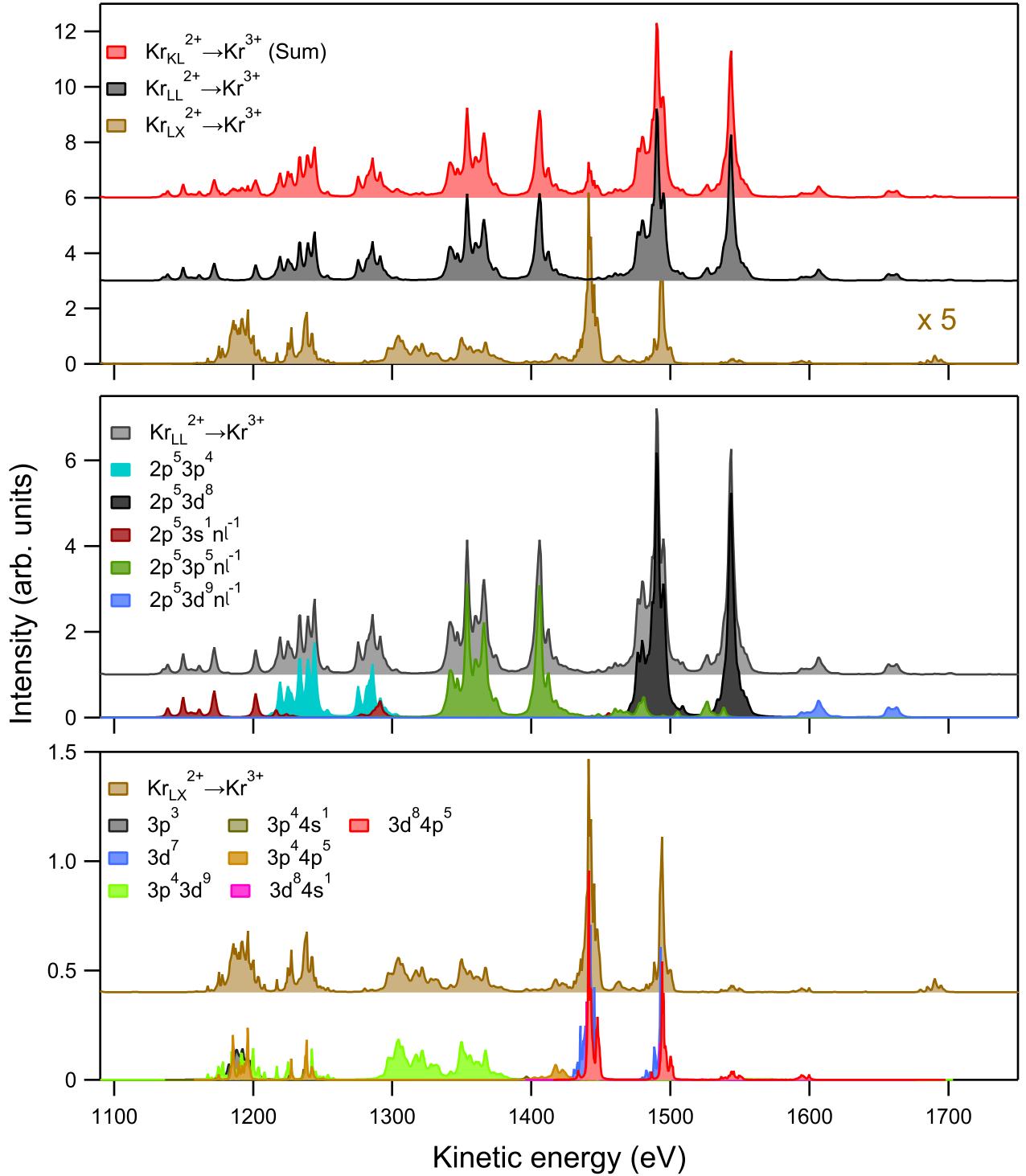
FIG. 5: Partial $Kr^{2+\prime} \rightarrow Kr^{3+\prime}$ contribution to total Auger spectrum after $1s$ ionization. The different colors in the lower part of each panel indicate contributions of transitions to individual final-state configurations.
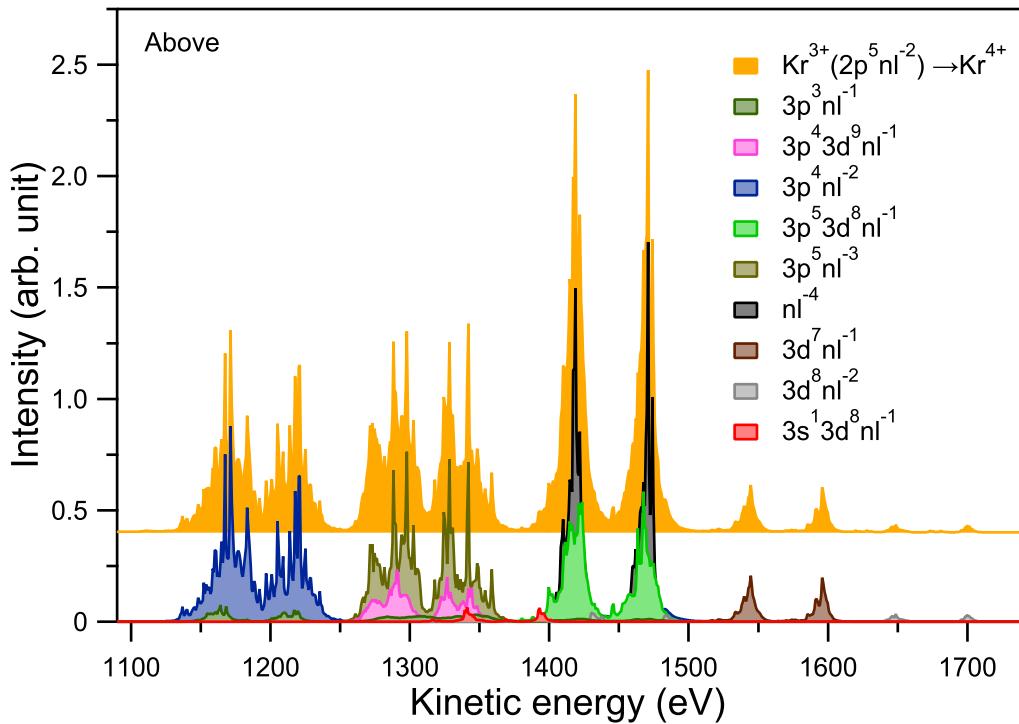
FIG. 6: Partial $Kr^{3+} \rightarrow Kr^{4+}$ contribution to total Auger spectrum after 1s ionization. The different colors in the lower part of indicate contributions of transitions to individual final-states configurations.

These triply charged ions can further decay via

$$\text{Kr}^{3+}(LXX) \rightarrow \text{Kr}^{4+}(XXXX) + e_{LXX-XXXX}. \quad (8)$$
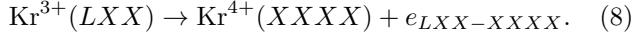
The partial Auger spectrum associated to $\text{Kr}^{3+} \rightarrow \text{Kr}^{4+}$ transitions is shown in Fig. 6. It corresponds to the decay of triply ionized states $2p^5 nl^{-2}$, where nl^{-2} represents doubly ionized $3p$ and $3d$ orbitals. The configurations of the quadruply ionized Kr final states are summarized in Table II.

It should be mentioned that the LL and LX initial states populated by KLL and KLX Auger can also decay via Coster-Kronig transitions, leading to even higher charged states. Here the mechanism is

$$\begin{aligned}
\text{Kr}^{2+}(L_1 L_1) &\rightarrow \text{Kr}^{3+}(L_1 L_{2,3} X) + e \\
&\rightarrow \text{Kr}^{4+}(L_{2,3} L_{2,3} XX) + e \quad (9) \\
&\rightarrow \text{Kr}^{5+}(L_{2,3} XXXX) + e
\end{aligned}$$
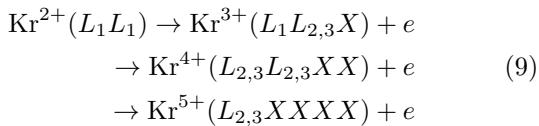
The last states can decay to Kr^{6+} or even to Kr^{7+}, if an additional $L_2 \rightarrow L_3 X$ Coster-Kronig decay occurs. However, since at each decay step the initial population spreads over an increasing amount of states, the spectra gradually smear into the background. Therefore these decays are not discussed further in the present work.

V. CONCLUSIONS

A detailled study of deep-core photoionization of Kr atoms has been presented, obtained by a hard X-ray photoelectron spectroscopy experiment, and supported by relativistic multiconfiguration interaction Dirac-Fock calculations. The core-hole lifetime of the Kr $1s$ orbital vacancy has been extracted; binding energies and relative intensities of the satellite structures have been also assigned. Furthermore, we show a detailed analysis of Auger cascade spectra below and above the $1s$ ionization threshold, starting from a singly ionized state, produced by both direct ionization and KL-emission processes, that undergoes further relaxation by Auger cascade leading to multiply ionized states. The role of the KL-emission versus KLL and KLX Auger emission on the creation of L-shell vacancies and on the Auger cascade intensities, due to the KL emission selection rule, has been stressed. As for the relaxation processes following the ionization of the $1s$ orbital, the KL-emission yields is determined to be 68%, which outweighs Auger emission yields estimated to 32%. $LX - LXX$ Auger structures have been revealed to be not negligible as is in the Xe case, and their intensities and energy positions have been assigned as results of the second-step KLL relaxation leading mostly to the creation of Kr^{3+} and Kr^{4+} ions. In addition to increasing the knowledge of the decay dynamics of medium-sized core-ionized ions, the work can be useful in investigations of molecules. As an example, the present experimental setup can be used to study electron and ion dynamics of core-ionized Br-containing molecules [31].

VI. ACKNOWLEDGEMENTS

[1] M. Oura, T. Gejo, K. Nagaya, Y. Kohmura, K. Tamasaku, L. Journel, M. N. Piancastelli and M. Simon, New Journal of Physics. **21**, 043015 (2019).

[2] J. C. Woicik, Hard X-ray photoelectron spectroscopy (HAXPES). (Springer Series in Surface Science vol 59) ed j Woicik (New York: Springer)(2016), and references therein.

[3] M. N. Piancastelli, K. Jänkälä, L. Journel, T. Gejo, Y. Kohmura, M. Huttula, M. Simon and M. Oura, Phys. Rev. A. **95**, 061402 (2017).

[4] N. Boudjemia, K. Jänkälä, T. Gejo, K. Nagaya, K. Tamasaku, M. Huttula, M. N. Piancastelli, M. Simon and M. Oura.Phys. Chem. Chem. Phys. **21**, 5448 (2019).

[5] J. Jauhiainen, A. Kivimäki, S. Aksela, O-P. Sairanen and H. Aksela, J. Phys. B: At. Mol. Opt. Phys. **28**, 4091 (1995).

[6] Y. Morishita, Y. Tamenori, K. Okada, K. Oyama, K. Yamamoto, K. Tabayashi, T. Ibuki, K. Moribayashi and I. H. Suzuki, J. Phys. B: At. Mol. Opt. Phys. **39**, 1323 (2006).

[7] I. H. Suzuki, A. Fujii, S. Nagaoka, M. Kosugi, K. Okada, T. Ibuki, S. Samori, Y. Tamenori and H. Ohashi, J. Phys. B: At. Mol. Opt. Phys. **37**, 1433 (2004).

[8] Eugene I. McGuire. Phy. Rev. A. **11**, 17 (1975).

[9] S. B. Hansen, K. B. Fournier, A. Ya. Faenov, A. I. Magunov, T. A. Pikuz, I. Yu. Skobelev, Y. Fukuda, Y. Akahane, M. Aoyama, N. Inoue, H. Ueda, and K. Yamakawa. Phys. Rev. E. **71**, 016408 (2005).

[10] M. Drescher, M. Hentschel, R. Kienberger, M. Uiberacker, V. Yakovlev, A. Scrinzi, Th. Westerwalbesloh, U. Kleineberg, U. Heinzmann and F. Krausz. Nature **419**, 803 (2002).

[11] J.F. Seely, C.A. Back, C. Constantin, R.W. Lee, H.-K. Chung, L.T. Hudson, C.I. Szabo, A. Henins, G.E. Holland, R. Atkin, L. Marlin. J. Quant. Spectrosc. Radiat. Transf **99**, 572-583 (2006).

[12] B. Rudek, D. Rolles, S. K. Son, L. Foucar, B. Erk, S. Epp, R. Boll, D. Anielski, C. Bostedt, S. Schorb, R. Cof-

fee, J. Bozek, S. Trippel, T. Marchenko, M. Simon, L. Christensen, S. De, S. W. K. Ueda, I. Schlichting, R. Santra, J. Ullrich, and A. Rudenko. Phys. Rev. A **87**, 023413 (2013).

[13] L. Young, D. A. Arms, E. M. Dufresne, R. W. Dunford, D. L. Ederer, C. Höhr, E. P. Kanter, B. Krässig, E. C. Landahl, E. R. Peterson, J. Rudati, R. Santra, and S. H. Southworth, Phys. Rev. Lett **97**, 083601 (2006).

[14] B. Krässig, J. C. Bilheux, R. W. Dunford, D. S. Gemmell, S. Hasegawa, E. P. Kanter, S. H. Southworth, L. Young, L. A. LaJohn, and R. H. Pratt, Phys. Rev. A **67**. 022707(2003).

[15] A. Filliponi, D. T. Bowron, C. Loban, and J. L. Finney, Phys. Rev. Lett. **79**, 1293 (1997).

[16] L. O. Werme, T. Bergmark. and K. Siegbahn, J. Physica Scripta. **6**, 2-3 141 (1972).

[17] K. Tamasaku, Y. Tanaka, M. Yabashi, H. Yamazaki, N. Kawamura, M. Suzuki and T. Ishikawa. Nucl. Instrum. Methods. A. **467-468**, 686 (2001).

[18] J. H. Hubbell, P. N. Trehan, N. Singh, B. Chand, D. Mehta, M. L. Grag, S. Singh, and S. Puri, J. Phys. Chem. Ref. Data **23**, 339 (1994), and references therein.

[19] The analyzer as well as the gas cell were originally supplied by Gammadata Scienta.

[20] L. Asplund, P. Kelfve, B, Blomster, H. Siegbahn, and K. Siegbahn, Phys, Scr. **16**, 268 (1977).

[21] R. D. Deslattes, E. G. Kessler, P. Indelicato, L. de Billy, E. Lindroth, and J. Anton, Rev. Mod. Phys, **75**, 35 (2003).

[22] M. F. Gu, Can. J. Phys **86**, 675 (2008).

[23] I. P. Grant. Springer Science & Business Media. **40**, (2007).

[24] J. Niskanen, K. Jänkälä, M. Huttula, and A. Föhlisch, J. Chem. Phys. **146**, 144312 (2017).

[25] K. G. Dyall. I. P. Grant, C. T. Johnson, F. A. Parpia, E. P. Plummer, GRASP: a general purpose relativistic atomic structure program, Comput. Phys. Commun. **55**, 425 (1989).

[26] I. P. Grant. J. Phys. B. **7**, 1458 (1974).

[27] M. O. Krause and J. H. Oliver, J. Phys. Chem. Ref. Data **8**, 329 (1979).

[28] O. Dragoun, A. Špalek, and F. Wuilleumier, Czech. J. Phys. **54**, 833 (2004).

[29] M. Breinig, M. H. Chen, G. E. Ice, F. Parente, B. Crasemann, and G. S. Brown, Phys. Rev. A **22**, 520 (1980).

[30] S. J. Schaphorst, A. F. Kodre, J. Ruscheinski, B. Crasemann, T. Åberg, J. Tulkki, M. Hsiung Chen, Y. Azuma and G. S. Brown, Phys. Rev. A. **47**, 1953 (1993).

[31] N. Boudjemia, *et al.*, Unpublished.